

## ***R*-band host galaxy contamination of TeV $\gamma$ -ray blazar Mrk 501: effects of the aperture size and seeing**

Hai-Cheng Feng<sup>1,2,3</sup>, Hong-Tao Liu<sup>1,3,4</sup>★, Ying-He Zhao<sup>1,3,4</sup>★, Jin-Ming Bai<sup>1,3,4</sup>, Fang Wang<sup>5</sup>, Xu-Liang Fan<sup>6</sup>

<sup>1</sup> Yunnan Observatories, Chinese Academy of Sciences, 396 Yangfangwang, Guandu District, Kunming, 650216, P. R. China

<sup>2</sup> University of Chinese Academy of Sciences, Beijing 100049, P. R. China

<sup>3</sup> Key Laboratory for the Structure and Evolution of Celestial Objects, Chinese Academy of Sciences, 396 Yangfangwang, Guandu District, Kunming, 650216, P. R. China

<sup>4</sup> Center for Astronomical Mega-Science, Chinese Academy of Sciences, 20A Datun Road, Chaoyang District, Beijing, 100012, P. R. China

<sup>5</sup> School of Physics and Space Science, China West Normal University, Nanchong, 637009, P. R. China

<sup>6</sup> School of Physics, Huazhong University of Science and Technology, Wuhan 430074, P. R. China

**Abstract** We simulated the *R*-band contribution of the host galaxy of TeV  $\gamma$ -ray BL Lac object Mrk 501 in different aperture sizes and seeing conditions. The intensive observations were run with the 1.02 m optical telescope at Yunnan Observatories from 2010 May 15 to 18. Based on the host subtraction data presented in Nilsson et al. (2007), the subtraction of host galaxy contamination results in significant seeing-brightness correlations. These correlations would lead to illusive large amplitude variations at short timescales, which will mask the intrinsic micro variability, thus gives rise to difficulty in detecting the intrinsic micro variability. Both aperture size and seeing condition influence the flux measurements, but aperture size impact the result more significantly. Based on the parameters of elliptical galaxy provided in Nilsson et al. (1999), we simulated the host contributions of Mrk 501 in the different aperture sizes and seeing conditions. Our simulation data of the host galaxy obviously weaken these significant seeing-brightness correlations for the host-subtracted brightness of Mrk 501, and can help us discover the intrinsic short timescale micro variability. The pure nuclear flux is  $\sim 8.0$  mJy in *R* band, i.e., AGN has a magnitude of  $R \sim 13^m.96$ .

**Key words:** galaxies: active — BL Lacertae objects: individual (Mrk 501)— techniques: photometric — methods: data analysis

### **1 INTRODUCTION**

Blazars are an extreme subclass of active galactic nuclei (AGNs), including BL Lacertae (BL Lac) objects and flat spectrum radio quasars (FSRQs) (e.g., Angel & Angel 1980; Urry & Padovani 1995; Fossati et al. 1998; Böttcher & Dermer 2002; Maraschi & Tavecchio 2003). They are characterized by rapid and strong variability over the whole electromagnetic spectrum, high and variable polarization from the optical to radio bands, and prominent non-thermal emission at all wavelengths. In general,

---

★ Corresponding authors: H. T. Liu, e-mail: htliu@ynao.ac.cn; Ying-He Zhao: zhaoyinghe@ynao.ac.cn.

these extreme properties can be generated from a relativistic jet with a viewing angle less than  $10^\circ$  (e.g., Blandford & Königl 1979; Urry & Padovani 1995). The broadband spectral energy distributions (SEDs) of blazars usually exhibit a double peak profile. The first component extends from infrared to ultraviolet or soft X-ray, and the second is located in the GeV/TeV gamma-ray bands (e.g., Ghisellini et al. 1998; Abdo et al. 2010). The first peak is generally believed to be the synchrotron radiation of relativistic electrons in the jet. The second peak is attributed to the inverse-Compton scattering of the same electron population that produces the synchrotron radiation (e.g., Dermer & Schlickeiser 1993; Böttcher 2007; Neronov et al. 2012).

Due to the property of strong variability of BL Lac object, the photometric technique is widely used to investigate the structure, radiation mechanism, dynamics, and the masses of the central supermassive black holes (e.g., Ciprini et al. 2003, 2007; Gupta et al. 2008a; Liu & Bai 2015; Dai et al. 2015). However, the host galaxies often exhibit strong radiation in the optical to near-infrared (NIR) bands. Thus, the contamination from the host galaxies may influence the photometric results, especially for nearby extended sources. The photometric aperture is either a dynamic aperture or a fixed aperture. The dynamic aperture could be a few times the seeing, and the case of an extended source will result in a significant dependence of the photometric magnitudes on the seeing. There is not the dependence on the seeing for a point source at high redshift. The fixed aperture and the dynamic aperture could result in similar influences on the photometric results for the extended source due to the seeing (see Feng et al. 2017). For point sources, the strong host galaxies could dilute the variability amplitudes of AGNs. Besides, the color indices and the SEDs of AGNs will be influenced. Since an extended source is resolved, different aperture sizes and seeing conditions would introduce large uncertainties in photometry at different epochs.

However, the host galaxies of nearby BL Lac objects are elliptical galaxies, which are huge (the effective radius  $R_e \sim 10$  kpc) and luminous ( $M_R \sim -24.^m0$ ) (e.g., Falomo & Kotilainen 1999; Urry et al. 1998, 2000; Scarpa et al. 2000; Kotilainen & Falomo 2004; Nilsson et al. 2003, 2007; Hyvönen et al. 2007). Even though some BL Lac objects may show signs of interaction with companions (e.g., Stickel et al. 1993; Falomo 1996; Heidt et al. 1999; Falomo & Ulrich 2000), there is no clear evidence in most cases that the nuclear activity is triggered by interaction (Nilsson et al. 1999, 2007). For most BL Lac objects, the morphologies of host galaxies are indistinguishable from the similar normal elliptical galaxies (Scarpa et al. 2000). Thus, the host galaxies of BL Lac objects can be simulated based on the normal elliptical galaxies.

Mrk 501 is a prototype nearby BL Lac object (redshift  $z = 0.034$ ), which has been widely studied over the two decades in the entire electromagnetic spectrum (e.g., Stickel et al. 1993; Quinn et al. 1996; Catanese et al. 1997; Samuelson et al. 1998; Xie et al. 1999, 2001; Konopelko et al. 2003; Gupta et al. 2008b, 2012; Albert et al. 2007; Abdo et al. 2011; Shukla et al. 2015; Ahnen et al. 2017). In the high energy regime from X-ray to TeV, Mrk 501 is one of the brightest extragalactic sources (Abdo et al. 2011). Many studies attempted to investigate its properties in the optical bands (e.g., Xie et al. 1999, 2001; Gupta et al. 2008b, 2012; Xiong et al. 2016). Based on the host subtraction data presented in Nilsson et al. (2007), widely used in the previous photometric studies, the subtraction of host galaxy contamination results in a significant seeing-magnitude correlation for Mrk 501 (Feng et al. 2017). The researches related to the variability will need a reasonable subtraction of the host galaxy, which should eliminate (partly) this significant seeing-brightness correlation.

In this paper, we presented observations of Mrk 501 in the  $R$  band from 2010 May 15 to 18. In order to obtain the host components in the different aperture radii and seeing conditions, we used the two-dimension simulation method to produce the host galaxy. The structure of this paper is as follows: Section 2 is the observations and data reduction; Section 3 gives the details of simulations; Section 4 is conclusions, and discussion is presented in Section 5.

## 2 OBSERVATIONS AND DATA REDUCTION

The observations of Mrk 501 was carried out with the 1.02 m optical telescope at Yunnan Observatories. This telescope is a classical Cassegrain telescope located at Kunming, China. An Andor AW436 CCD

**Table 1** Observation log and results of IDV observations of Mrk 501.

Date	N	Exposure (s)	$\sigma(\text{star1-star6})$
2010 May 15	88	150	0.005
2010 May 16	88	150	0.007
2010 May 17	80	150	0.005
2010 May 18	70	150	0.005

Notes: Column 1: observation dates; Column 2: observation numbers; Column 3: exposure time; Column 4: standard deviation of the (star 1 - star 6).

(2048 pixels  $\times$  2048 pixels) camera was equipped at the  $f/13.3$  Cassegrain focus of the 1.02 m telescope. The entire field of view of the CCD is  $\sim 7.3 \times 7.3$  arcmin<sup>2</sup>, and each pixel corresponds to 0.21 arcsec in both dimensions. The CCD readout noise and gain are 6.33 electrons and 2.0 electrons/ADU, respectively (e.g., Dai et al. 2015; Xiong et al. 2016). We selected the standard Johnson broadband filters to carry out the observations in the  $R$  band, and 326 valid exposures were obtained in 4 nights from 2010 May 15 to 2010 May 18. The exposure time is 150 seconds for each frame. Table 1 presents the complete observation log. For each image, the standard stars are always in the same field with the object.

Because the magnitudes of the standard stars are considered constant, the brightness of the object could be calibrated using the standard stars (e.g., Bai et al. 1998; Fan et al. 2014; Zhang et al. 2004, 2008). There are 6 standard stars, whose magnitudes have been measured in other works, in the field. (Villata et al. 1998; Fiorucci & Tosti 1996). In order to improve the measurement accuracy of the object magnitude, the selection of the standard stars should consider both of the position in the field and the brightness. Star 1 is the brightest of all nearby standard stars [see Figure 9 in Villata et al. (1998) for numbering], and is very close to the object. Thus, we selected star 1 to calculate the object magnitude. However, there are some uncertainties, which may introduce some errors to the standard stars, i.e. the relative brightness of the standard stars may change in some images. So another comparison star is necessary. Star 6 is the closest to the object, and is used as another standard star. We used the standard deviation of the star 1 and star 6 [ $\sigma(\text{star1-star6})$ ] to characterize the change. The standard deviation of the differential instrumental magnitude of star1-star6 is  $\sim 0.005$  (see Table 1).

All of the observed data was reduced using the standard procedure in the Image Reduction and Analysis Facility (IRAF) software. For each night, we took the median of all the bias frames and generated a master bias. Then the master bias was subtracted from all the object image frames and flat-field image frames. We used the same method to generate the master flat-field, and then the flat-field correction was performed. After the corrections of bias and flat-field, aperture photometry was performed using the APPHOT task. Considering the standard stars are point sources, an extraction aperture depending on full width at half maximum (FWHM), i.e., a dynamic aperture, was used to obtain the maximum signal-to-noise ratio (S/N) (Howell 1989). We found that the best S/N was obtained with the aperture radius of 1.2 FWHM [minimizing  $\sigma(\text{star1-star6})$ ]. For the target, we chose 19 fixed aperture radii from 1 arcsec to 10 arcsec to investigate the property of the host galaxy. The epoch, differential magnitude, and FWHM of each image are listed in Tables 2-5. Figure 1 shows the relationship between the FWHMs and the magnitudes in different apertures for each night, and Figure 2 shows the corresponding relationship of the FWHMs and the fluxes. Figures 1 and 2 indicate that both of the FWHM and aperture affect the photometric results. The brightness increases as the aperture increases, and decreases as the seeing increases. The increasing aperture will contain more light, and the increasing seeing will scatter more light out of the aperture.

### 3 SIMULATIONS OF HOST GALAXY

The host galaxy of Mrk 501 is an elliptical galaxy (e.g., Nilsson et al. 1999, 2003; Hyvönen et al. 2007). Thus, we simulated the host galaxy using a two-dimensional model, which assumes the surface brightness  $I(r)$  follows the Sérsic law  $\sim r^\beta$  (Sérsic 1968; Caon et al. 1993; Nilsson et al. 1999). The

**Table 2** The observed data on 2010 May 15

MJD (day)	Apert													FWHM (arcsec)	
	1.0	1.5	2.0	2.5	3.0	3.5	4.0	4.5	5.0	5.5	6.0	6.5	...		10.0
5331.699363	4.121	6.985	9.483	11.412	12.958	14.235	15.239	16.179	16.988	17.740	18.423	19.044	...	22.416	1.98
5331.701875	4.335	7.214	9.651	11.581	13.102	14.353	15.380	16.299	17.114	17.871	18.542	19.167	...	22.519	1.86
5331.703727	4.307	7.174	9.597	11.475	12.970	14.182	15.183	16.105	16.926	17.642	18.287	18.904	...	22.128	1.89
5331.705590	4.256	7.147	9.588	11.486	12.970	14.195	15.197	16.105	16.910	17.642	18.287	18.886	...	22.088	1.93
5331.707442	4.271	7.167	9.615	11.496	12.994	14.222	15.211	16.105	16.895	17.610	18.271	18.904	...	22.190	1.90
5331.711146	4.056	6.921	9.448	11.433	13.006	14.287	15.323	16.254	17.082	17.789	18.474	19.096	...	22.374	2.00
...	...	...	...	...	...	...	...	...	...	...	...	...	...	...	...
5331.692500	3.950	6.776	9.293	11.276	12.840	14.156	15.183	16.149	16.973	17.724	18.406	19.009	...	22.272	2.00

Notes: This table is available in its entirety in a machine-readable form in the online journal. A portion is shown here for guidance regarding its form and content. MJD = JD - 2450000. Apert: aperture radius in units of arcsec, presented in columns 2–15. The fluxes are in unit of mJy.

**Table 3** The observed data on 2010 May 16

MJD (day)	Apert													FWHM (arcsec)	
	1.0	1.5	2.0	2.5	3.0	3.5	4.0	4.5	5.0	5.5	6.0	6.5	...		10.0
5332.644491	3.160	5.719	8.169	10.227	11.829	13.139	14.156	15.071	15.869	16.586	17.241	17.855	...	21.152	2.63
5332.647292	3.349	5.994	8.483	10.475	12.027	13.272	14.274	15.197	15.972	16.663	17.288	17.871	...	20.881	2.38
5332.649294	3.383	6.050	8.514	10.456	11.983	13.211	14.195	15.071	15.840	16.541	17.161	17.740	...	20.785	2.40
5332.651157	3.446	6.123	8.633	10.660	12.273	13.557	14.580	15.508	16.329	17.051	17.675	18.271	...	21.308	2.27
5332.653009	3.501	6.202	8.681	10.689	12.262	13.519	14.553	15.479	16.284	17.004	17.626	18.237	...	21.328	2.28
5332.654861	3.282	5.907	8.405	10.427	12.038	13.346	14.393	15.309	16.105	16.833	17.480	18.070	...	21.210	2.45
...	...	...	...	...	...	...	...	...	...	...	...	...	...	...	...
5332.829722	3.782	6.543	9.040	10.999	12.524	13.771	14.769	15.651	16.434	17.146	17.805	18.389	...	21.506	2.13

Notes: This table is available in its entirety in a machine-readable form in the online journal. A portion is shown here for guidance regarding its form and content. MJD = JD - 2450000. Apert: aperture radius in units of arcsec, presented in columns 2–15. The fluxes are in unit of mJy.

**Table 4** The observed data on 2010 May 17

MJD (day)	Apert													FWHM (arcsec)	
	1.0	1.5	2.0	2.5	3.0	3.5	4.0	4.5	5.0	5.5	6.0	6.5	...		10.0
5333.686539	4.079	6.921	9.370	11.245	12.734	13.924	14.906	15.782	16.571	17.256	17.888	18.474	...	21.565	2.01
5333.688796	4.053	6.902	9.327	11.183	12.617	13.771	14.728	15.565	16.329	17.004	17.610	18.187	...	21.289	2.05
5333.690648	3.803	6.591	9.081	11.009	12.524	13.745	14.742	15.637	16.419	17.114	17.773	18.338	...	21.486	2.19
5333.692500	3.931	6.745	9.174	11.050	12.501	13.695	14.634	15.494	16.254	16.926	17.529	18.086	...	21.074	2.13
5333.694352	3.761	6.543	9.006	10.898	12.341	13.532	14.486	15.337	16.090	16.755	17.352	17.904	...	20.843	2.18
5333.696215	4.193	7.069	9.492	11.338	12.757	13.911	14.837	15.680	16.419	17.082	17.707	18.271	...	21.250	1.98
...	...	...	...	...	...	...	...	...	...	...	...	...	...	...	...
5333.836632	3.645	6.382	8.883	10.928	12.547	13.860	14.947	15.898	16.755	17.529	18.203	18.834	...	22.128	2.17

Notes: This table is available in its entirety in a machine-readable form in the online journal. A portion is shown here for guidance regarding its form and content. MJD = JD - 2450000. Apert: aperture radius in units of arcsec, presented in columns 2–15. The fluxes are in unit of mJy.

formula of  $I(r)$  is

$$I(r) = I(r_e) \operatorname{dex} \left\{ -b_\beta \left[ \left( \frac{r}{r_e} \right)^{-\beta} - 1 \right] \right\}, \quad (1)$$

**Table 5** The observed data on 2010 May 18

MJD (day)	Apert													FWHM (arcsec)	
	1.0	1.5	2.0	2.5	3.0	3.5	4.0	4.5	5.0	5.5	6.0	6.5	...		10.0
5334.700336	3.717	6.489	8.949	10.858	12.387	13.607	14.593	15.494	16.299	17.020	17.691	18.304	...	21.525	2.19
5334.702801	3.530	6.225	8.689	10.699	12.296	13.607	14.674	15.623	16.465	17.225	17.904	18.508	...	21.765	2.27
5334.704664	4.019	6.838	9.301	11.255	12.804	14.065	15.099	16.031	16.864	17.626	18.287	18.921	...	22.251	1.99
5334.706516	3.782	6.561	9.023	10.958	12.478	13.720	14.715	15.608	16.404	17.098	17.756	18.355	...	21.525	2.12
5334.708368	3.772	6.543	9.006	10.969	12.536	13.796	14.823	15.753	16.556	17.288	17.970	18.576	...	21.805	2.14
5334.710231	3.619	6.323	8.801	10.788	12.409	13.733	14.796	15.767	16.632	17.384	18.070	18.713	...	22.006	2.17
...	...	...	...	...	...	...	...	...	...	...	...	...	...	...	...
5334.833229	3.652	6.400	8.883	10.828	12.352	13.594	14.607	15.522	16.329	17.051	17.691	18.287	...	21.545	2.19

Notes: This table is available in its entirety in a machine-readable form in the online journal. A portion is shown here for guidance regarding its form and content. MJD = JD - 2450000. Apert: aperture radius in units of arcsec, presented in columns 2–15. The fluxes are in unit of mJy.

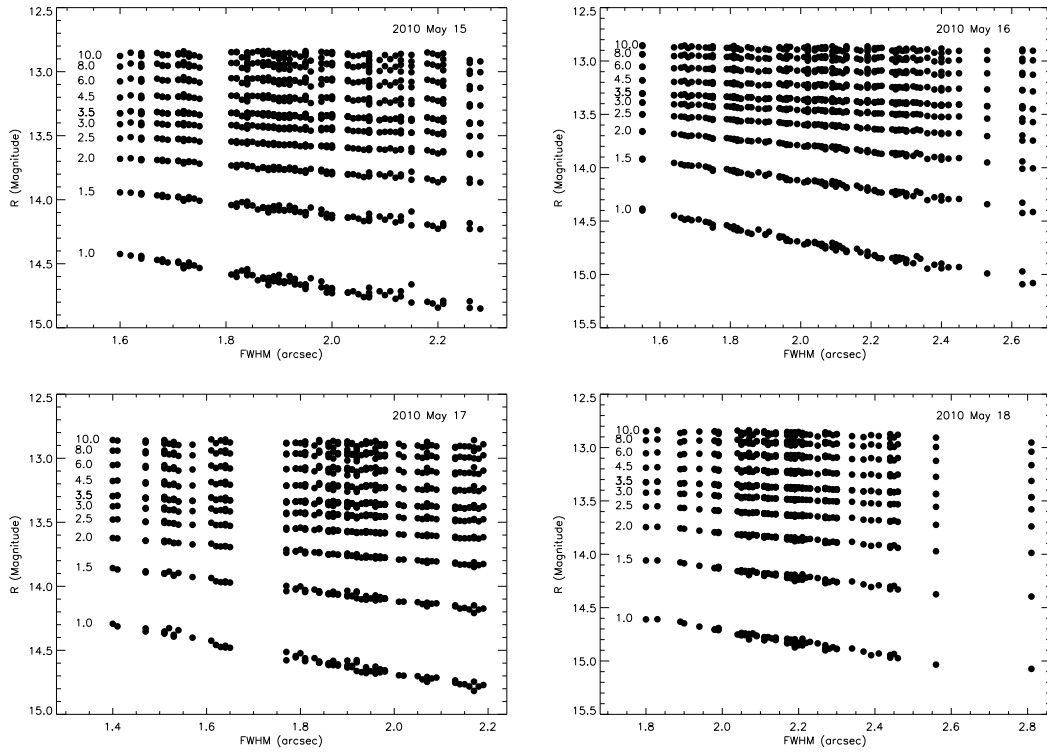


**Fig. 1** The relationships between FWHM and magnitude for different photometric aperture radii in our observations.

where  $\beta$  is the shape parameter,  $r_e$  is the effective radius (containing half of the total luminosity), a  $\beta$ -dependent constant  $b_\beta$  is defined as

$$b_\beta = \frac{0.868}{\beta} - 0.142, \quad (2)$$

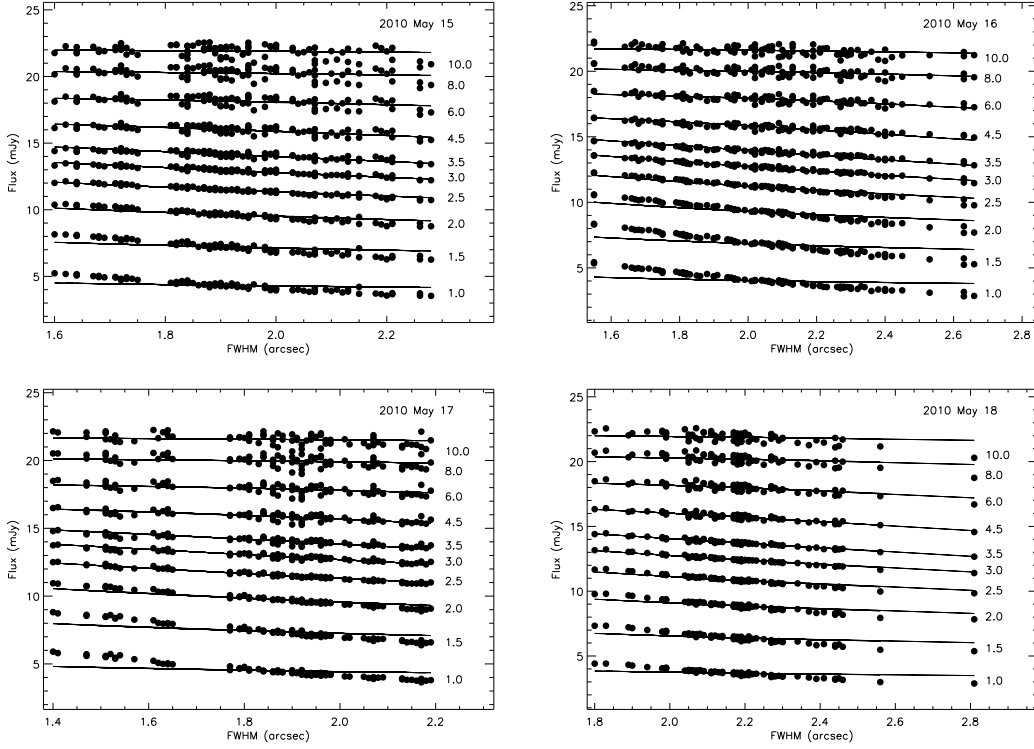


**Fig. 2** The relationships between FWHM and flux for different photometric aperture radii in our observations. The solid lines are the simulations vertically moved by the average differences between the original simulations and the corresponding observational data (the solid circles).

and

$$I(r_e) = \frac{f_R}{K_\beta r_e^2 (1 - \epsilon)}, \quad (3)$$

where  $f_R$  is the total flux of the galaxy,  $\epsilon$  is the ellipticity, and  $K_\beta$  can be derived from

$$K_\beta = dex(0.030 \log^2 \beta - 0.441 \log \beta + 1.079), \quad (4)$$

where  $dex$  means  $dex(x) = 10^x$ . Equations (1) to (4) indicate that if we obtained the parameters of  $\beta$ ,  $\epsilon$ ,  $r_e$ , and  $f_R$ , we could confirm the surface brightness  $[I(r)]$  distribution of the host galaxy. Combining with the position angle  $\theta$ , we can simulate the host of Mrk 501 in the observed images. However, the lower resolution and the relatively poor S/N restrict us to measure the accurate values of the above parameters. Fortunately, Nilsson et al. (1999) has obtained all the above parameters from the high-resolution images in the  $R$  band. The free  $\beta$  + core model was adopted in our simulations [based on the properties of BL Lac objects and the de Vaucouleurs model (e.g., Makino et al. 1990)]. We simulated the host component of Mrk 501, and convolved the simulation results into 28 different FWHMs with the point spread function (PSF) of Gaussian profile. The FWHMs of the convolved images are from 0.5 to 5.9 arcsec with a bin size of 0.2 arcsec. We performed the photometry using 111 fixed apertures from 1.0 to 12.0 arcsec with a bin size of 0.1 arcsec. Table 6 shows the flux simulations for the host galaxy under different FWHMs and apertures. Figure 3 shows the relationship among the brightness, FWHMs,

**Table 6** The simulation data for host galaxy of Mrk 501

Apert	FWHM														
	0.5	0.7	0.9	1.1	1.3	1.5	1.7	1.9	2.1	2.3	2.5	2.7	2.9	...	5.9
1.0	2.615	2.138	1.732	1.425	1.190	1.012	0.872	0.762	0.672	0.599	0.537	0.486	0.441	...	0.164
1.1	2.928	2.456	2.023	1.681	1.413	1.207	1.043	0.913	0.806	0.719	0.646	0.585	0.532	...	0.199
1.2	3.231	2.775	2.322	1.949	1.649	1.415	1.226	1.076	0.951	0.850	0.764	0.692	0.630	...	0.236
1.3	3.512	3.082	2.620	2.222	1.893	1.632	1.419	1.249	1.106	0.990	0.891	0.808	0.736	...	0.277
1.4	3.782	3.383	2.920	2.503	2.147	1.860	1.623	1.431	1.271	1.139	1.026	0.931	0.849	...	0.321
1.5	4.034	3.668	3.213	2.783	2.405	2.095	1.834	1.622	1.443	1.296	1.168	1.062	0.969	...	0.368
...	...	...	...	...	...	...	...	...	...	...	...	...	...	...	...
12.0	15.554	15.542	15.527	15.509	15.486	15.460	15.429	15.394	15.354	15.311	15.259	15.206	15.143	...	12.889

Notes: This table is available in its entirety in a machine-readable form in the online journal. A portion is shown here for guidance regarding its form and content. Apert: aperture radius in units of arcsec, presented in column 1. FWHM is in units of arcsec, presented in columns 2–16. The fluxes are in unit of mJy.

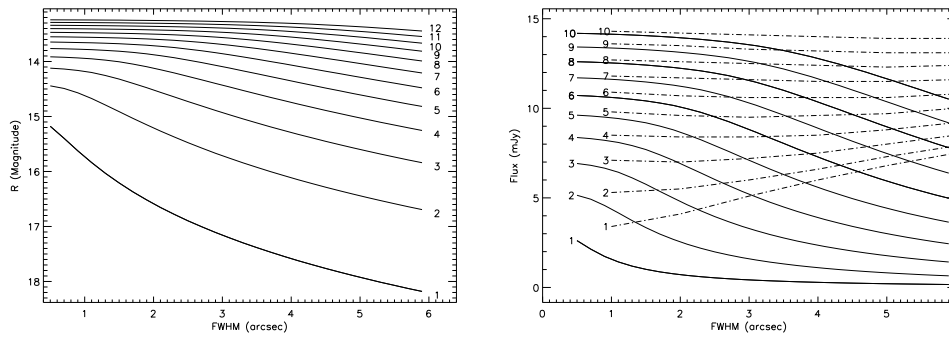


**Fig. 3** The relationships between FWHM and brightness for different apertures in simulation to the host galaxy of Mrk 501 (the solid lines). The dotted-dashed lines represent the results of Nilsson et al. (2007). The numbers following the lines in plots are the photometric aperture radii.

and apertures. Our simulation results are very different from those in Nilsson et al. (2007). The host subtraction based on the subtraction data in Nilsson et al. (2007) led to a significant seeing-brightness correlation for Mrk 501 (see an example presented in Figure 2 in Feng et al. 2017). Thus, a reasonable host subtraction is needed for the optical photometry for Mrk 501.

We used two methods to compare the simulation results with our observations. First, we checked the observed images to determine photometric regions where the S/N ratios are high enough (i.e.,  $> 5$ ). This is normally achieved with an aperture radius of 5 arcsec. We measured the brightness of the images within annular apertures with radii of 3.5–4.5 and 4.5–5.0 arcsec. Figure 4 shows the comparisons between the simulated and observed results in the same annular apertures. The simulations and observations are (marginally) consistent with each other in the case of 3.5–4.5 arcsec except for 2010 May 17 (see Figure 4). In general, the observed results are less than the simulation results in the case of 4.5–5.0 arcsec. This may rise from low S/N ratios at those annular apertures. The host galaxy of Mrk 501 is a low surface brightness galaxy, and this will result in lower S/N ratios at larger annular apertures. The deviations of simulations from observations in the case of 3.5–4.5 arcsec are less than those in the case of 4.5–5.0 arcsec. Combing four panels in Figure 4 into one panel (see Figure 5), we find that simulations are marginally consistent with observations in the case of 3.5–4.5 arcsec, and the deviations of observations from simulations in the case of 3.5–4.5 arcsec are less than those in the case of 4.5–5.0

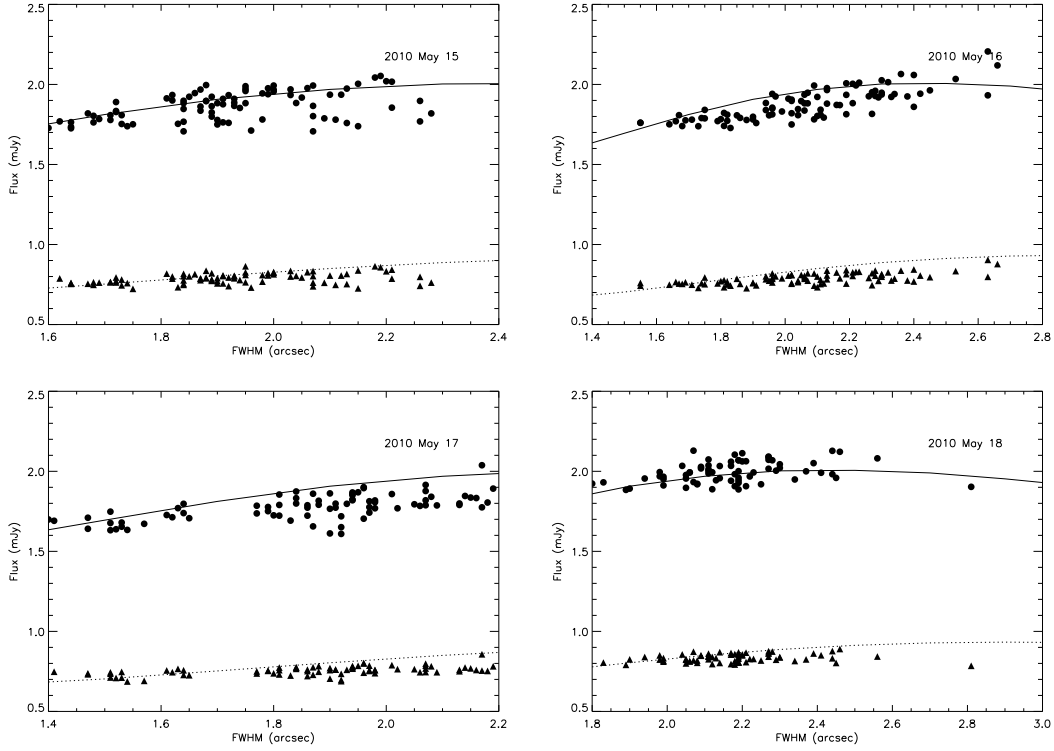


**Fig. 4** Fluxes in annular apertures for different seeing (FWHM). In each panel, the solid line denotes the simulation results from 3.5 to 4.5 arcsec, and the circles denote the observed results in the same annular apertures. In each panel, the dotted line denotes the simulation results from 4.5 to 5.0 arcsec, and the triangles denote the observed results in the same annular apertures.

arcsec. Observations need an exposure time to obtain a certain  $S/N$  ratio. A low  $S/N$  ratio may result in a lower flux measurement compared to the flux simulation based on a high  $S/N$  ratio image presented in Nilsson et al. (1999). Another method is based on the fact that the brightness difference between simulation and observation is the contribution of AGN, i.e., the observed flux is a combination of AGN and its host galaxy flux, while the simulation result only contains the host component. For a relatively large photometric aperture (nearly including all the AGN flux, e.g., an aperture radius of 4.0 arcsec including 99% of the AGN flux), the differences between simulations and observations should be a constant for the different seeing conditions. The observed results are well consistent with the vertically shifted simulation results for the aperture radii from 3.0 to 6.0 arcsec in the flux versus FWHM diagram (see Figure 2). There are very similar trends between the vertically shifted simulations and the observational results for the other aperture radii in Figure 2. These slight differences between simulations and observations may be from the fact that the corresponding aperture radii are either too small or too large ( $<3.0$  or  $>6.0$  arcsec).

We calculated the average difference between the simulations and the observational results in Figure 2. The shifted simulation results are well consistent with the observational data, and the average difference can be regarded as the AGN flux. The mean flux of AGN is  $\sim 8.0$  mJy, which corresponds to  $R \sim 13^m 96$  [ $F = 3.08 \times 10^{-0.4 \times R + 3}$  Jy (Nilsson et al. 2007)]. Thus, AGN's contribution to the



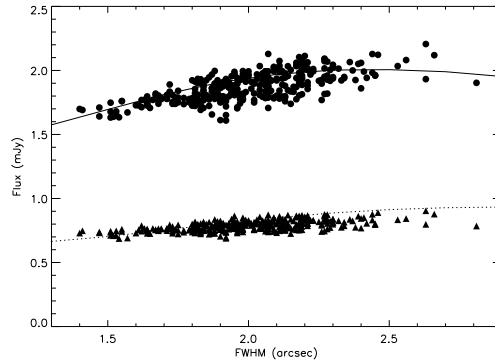


**Fig. 5** These observational fluxes on 2010 May 15 – 18. The symbols are same as in Figure 4.

total flux of the source is  $\sim 13.3\%$ . Compared with the brightness obtained in Nilsson et al. (1999),  $R = 14^m45$ , AGN Mrk 501 brightened by  $\sim 57\%$  in our observations. According to our simulations, we subtracted the host contribution, and investigated whether there are still significant seeing-brightness correlations for AGN Mrk 501. The host-subtracted fluxes versus FWHMs are presented in Figure 6. There is no correlation on 2010 May 18. Though the host-subtraction based on our simulations can (obviously) weaken the significant correlations found in Feng et al. (2017), there are still correlations for 2010 May 15 and 17, and an obvious correlation on 2010 May 16. Figure 7 shows the host-subtracted flux versus seeing distribution in the case of 5.0 arcsec aperture. The host-subtracted flux versus seeing distribution shows that the larger photometric aperture radii can further weaken the host-subtracted brightness-seeing correlation. Thus, our simulations can basically give a reasonable host-subtraction. The obvious correlation on 2010 May 16 might be from the smaller photometric aperture relative to the average seeing. The host-subtracted flux light curves show that the darkening variations found in Feng et al. (2017) still exist in the light curve on 2010 May 15 even though the host contribution has been subtracted (see Figure 8). There is a flare with a duration  $\sim 1$  hours on 2010 May 18 around MJD 5334.75 (see Figure 8), which was not found in Feng et al. (2017). This confirms that the fake large amplitude fast variability due to the seeing effect can mask the intrinsic micro variability in Mrk 501. This kind of fake rapid and strong variability due to seeing effect will mask the intrinsic micro variability in Mrk 501, and will lead to difficulty in detecting the intrinsic micro variability in similar sources with brighter host galaxies, e.g., Mrk 421.

#### 4 CONCLUSIONS

Based on the intensive observations run with the 1.02 m optical telescope at Yunnan Observatories from 2010 May 15 to 18, and a two-dimensional model of elliptical galaxy, we simulated the  $R$ -band contribution of the host galaxy of TeV  $\gamma$ -ray BL Lac object Mrk 501. The simulated brightness in the different aperture radii and seeing conditions shows correlations between the seeing and brightness for the host galaxy, and these correlations are well confirmed by the observational data. The differences between the simulation fluxes and the observational data are due to AGN Mrk 501 contribution, and the host-subtracted brightness of Mrk 501 can obviously weaken these significant correlations found in Feng et al. (2007). There is no correlation between the seeing and the host-subtracted brightness on 2010 May 18. However, there are correlations on 2010 May 15 and 17, and an obvious correlation on 2010 May 16. The larger photometric aperture radii with respect to the seeing average can further weaken the correlation on 2010 May 16 (see Figures 6 and 7). These correlations led to illusive large

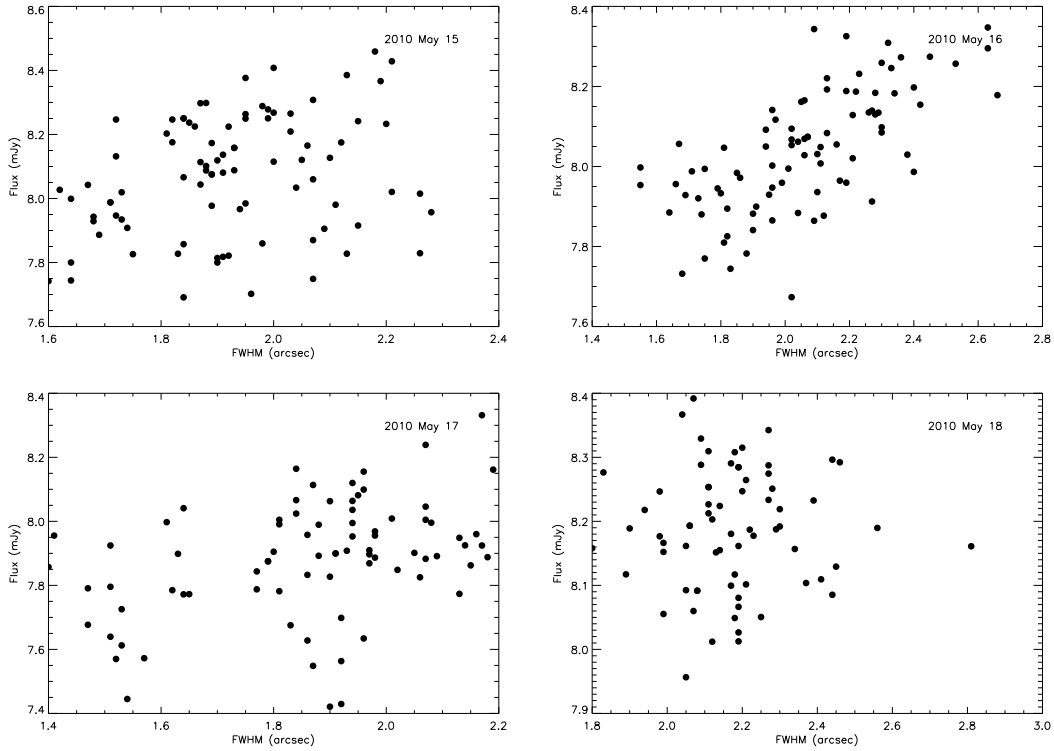


**Fig. 6** AGN host-subtracted flux versus seeing (FWHM). The observed fluxes are measured for the photometric aperture radius of 4.0 arcsec.

amplitude variations on short timescales, which can mask the intrinsic micro variability and then lead to the difficulty in detecting the intrinsic micro variability. The host-subtracted brightness light curves confirm the darkening variations on 2010 May 15 found in Feng et al. (2017), and discover a flare with a duration  $\sim 1$  hours on 2010 May 18. Both of the aperture size and the seeing condition influence the photometric results, but the aperture size can generate a more serious influence. The pure nuclear flux is  $\sim 8.0$  mJy. Compared with the result observed in 1996 July (Nilsson et al. 1999), the AGN Mrk 501 brightened by a factor of  $\sim 57\%$ . Simulation data of the host galaxy of Mrk 501 are given for the different aperture radii and seeing conditions (on-line Table 6).

## 5 DISCUSSION

The correlation between the seeing FWHM and the brightness within a certain aperture is obvious for the intensive observations on 2010 May 15 to 18. At the same time, the flux of the target is higher as the aperture radius is larger. The larger aperture radius will cover a more area of an extended source, and then will contain more light in the aperture. Thus, the total brightness will be monotonously increasing with the aperture radius. This indicates that a fixed aperture is better than a dynamic aperture in performing photometry for Mrk 501. This point was tested in Feng et al. (2017), where a fixed aperture was used to perform photometry. Brightness monotonously decreases with the increasing FWHM of seeing in the fixed aperture. This can be explained that the larger PSF due to the worse seeing will scatter out more light from a fixed aperture. Another feature is that the PSF effect is more significant for the smaller aperture (less than 3.0 arcsec). This is due to the fact that the scattered light of AGN changes for the

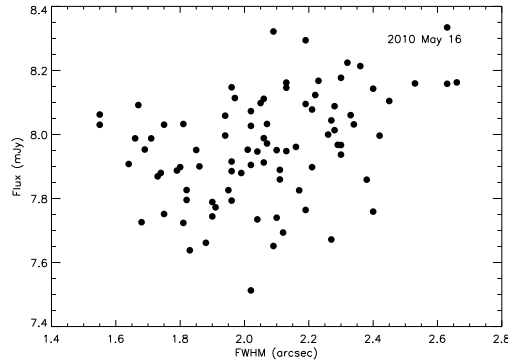


**Fig. 7** AGN host-subtracted flux versus seeing (FWHM) on 2010 May 16 for an aperture radius of 5.0 arcsec.

different PSFs. Therefore, the photometry of Mrk 501 should use a large fixed aperture, which can contain almost all the light of the AGN. In addition, it is necessary to correct the influence of seeing.

Figure 3 shows the simulation results of the host galaxy of Mrk 501, and the two panels in Figure 3 present the similar relationships in Figures 1 and 2. The brightness curve shapes of simulation results are very similar to those of observations for the same aperture and the same range of FWHM. However, the results in Figure 3 are somewhat different from the results in Figures 1 and 2, especially in the small apertures, and this difference is mainly due to the AGN component. We tested the reliability of the simulations via two methods (see Section 3), and both tests indicate that the simulations are robust (see Figure 2). The results in Figure 3 can be used to correct the host contamination of Mrk 501, and the corresponding values are given in Table 6. Nilsson et al. (2007) had given a similar table (Table B.1). Comparing our simulation results to theirs (see Figure 3), we found some differences. Though these two results indicate that the host fluxes depend strongly on the photometric apertures, the values from the same aperture and PSF are inconsistent. Especially within small aperture radius ( $\leq 3.0$  arcsec), the difference is significant. For a fixed aperture, the relationships between brightness and FWHM are significantly different for these two results. The brightness of the host galaxy decreases as the FWHM increases (see Figure 3). These trends are opposite to the results in Nilsson et al. (2007). The influence of the seeing on the variability amplitude is significant in our results. After we subtracted the contamination of the host galaxy using the results of Nilsson et al. (2007), the relationships are still significant for the brightness and seeing FWHM. Otherwise, if the brightness of the host galaxy monotonously increases with the FWHM, the outer part of the host galaxy would be brighter than the central part. This is inconsistent with the universal of the surface brightness distribution of elliptical galaxy.

The simulations and observations indicate that the AGN contribution of Mrk 501 is  $\sim 13.3\%$ . This means that even the variable of AGN is up to 10%, we can only detect a magnitude change  $\sim 0.^m01$  for the whole galaxy. This variability amplitude approximates to the limit accuracy of photometry for some telescopes. Therefore, it is not easy in detecting this variability in Mrk 501. The effects of the photometric aperture and the observational seeing are significant for the photometric results, and most of the previous works didn't take into account the effects of the two factors. This might lead to some fake variability in some previous works for Mrk 501, and the relevant results should be reconsidered. Our studies suggest that a fixed aperture, which depends on the seeing condition, is better than a dynamic aperture, and the host galaxy subtraction is necessary. Our simulations give a reasonable host-subtraction. The strong host contamination also impact the color, polarization, and SED of AGN. Thus, it is meaningful to subtract the host component before investigating the property of Mrk 501.

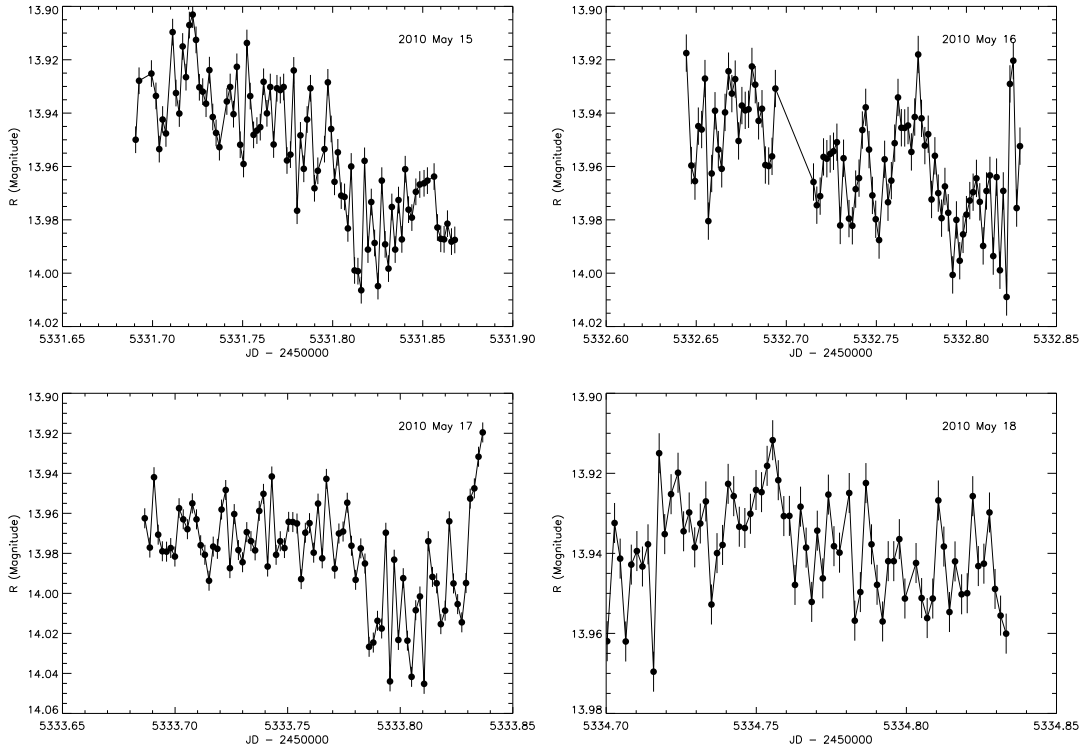


**Fig. 8** AGN host-subtracted light curves for a photometric aperture radius of 4.0 arcsec.

**Acknowledgements** We are grateful to the anonymous referee for constructive comments leading to significant improvement of this paper, and the editor for helpful suggestions. We thank the financial supports of the Key Research Program of the CAS (Grant No. KJZD-EW-M06), the National Natural Science Foundation of China (NSFC; Grant No. 11433004), and the Ministry of Science and Technology of China (2016YFA0400700). We also thank the financial supports of the NSFC (Grants No. 11273052 and U1431228), and the Youth Innovation Promotion Association, CAS.

## References

- Abdo, A. A., Ackermann, M., Agudo, I., et al. 2010, *ApJ*, 716, 30  
 Abdo, A. A., Ackermann, M., Ajello, M., et al. 2011, *ApJ*, 727, 129  
 Ahnen, M. L., Ansoldi, S., Antonelli, L. A., et al. 2017, *A&A*, 603, A31  
 Albert, J., Aliu, E., Anderhub, H., et al. 2007, *ApJ*, 669, 862  
 Angel, J. R. P. & Stockman, H. S. 1980, *ARA&A*, 18, 321  
 Bai, J. M., Xie, G. Z., Li, K. H., et al. 1998, *A&AS*, 132, 83B  
 Blandford, R., D., & Königl, A. 1979, *ApJ*, 232, 34  
 Böttcher, M., & Dermer, C. D. 2002, *ApJ*, 564, 86  
 Böttcher, M. 2007, *Ap&SS*, 309, 95  
 Caon, N., Capaccioli, M., & D'Onofrio, M. 1993, *MNRAS*, 265, 1013  
 Catanese, M., Bradbury, S. M., Breslin, A. C., et al. 1997, *ApJ*, 487, 143  
 Catanese, M., & Sambruna, R. M. 2000, *ApJL*, 534, L39  
 Ciprini, S., Tosti, G., Raiteri, C. M., et al. 2003, *A&A*, 400, 487

- Ciprini, S., Takalo, L. O., Tosti, G., et al. 2007, *A&A*, 467, 465  
Dai, B. B., Zeng, W., Jiang, Z. J., et al. 2015, *ApJS*, 218, 18  
Dermer, C. D., & Schlickeiser, R. 1993, *ApJ*, 416, 458  
Falomo, R. 1996, *MNRAS*, 283, 241  
Falomo, R., & Kotilainen, J. 1999, *A&A*, 352, 85  
Falomo, R., & Ulrich, M.-H. 2000, *A&A*, 357, 91  
Fan, J. H., Kurtanidze, O., Liu, Y., et al. 2014, *ApJS*, 213, 26  
Feng, H. C., Liu, H. T., Bai, J. M., et al. 2017, *ApJ*, 849, 161  
Fiorucci, M., & Tosti, G. 1996, *A&AS*, 116, 403  
Fossati, G., Maraschi, L., Celotti, A., et al. 1998, *MNRAS*, 299, 433  
Ghisellini, G., Celotti, A., Fossati, G., et al. 1998, *MNRAS*, 301, 451  
Gupta, A. C., Fan, J. H., Bai, J. M., et al. 2008a, *ApJ*, 135, 1384  
Gupta, A. C., Deng, W. G., Joshi, U. C., Bai, J. M., & Lee, M. G. 2008b, *NewA*, 13, 375  
Gupta, S. P., Pandey, U.S., Singh, K., et al. 2012, *NewA*, 17, 8  
Heidt, J., Nilsson, K., Sillanpää, A., et al. 1999, *A&A*, 341, 683  
Howell, S. B. 1989, *PASP*, 101, 616  
Hyvönen, T., Kotilainen, J. K., Falomo, R., et al. 2007, *A&A*, 476, 723  
Konopelko, A., Mastichiadis, A., & Kirk, J. 2003, *ApJ*, 597, 851  
Kotilainen, J., & Falomo, R. 2004, *A&A*, 424, 107  
Liu, H. T., & Bai, J. M., 2015, *AJ*, 149, 191  
Makino, J., Akiyama, K., & Sugimoto, D. 1990, *PASJ*, 42, 205  
Maraschi, L., & Tavecchio, F., 2003, *ApJ*, 593, 667  
Neronov, A., Semikoz, D., & Taylor, A. M. 2012, *A&A*, 541, 31  
Nilsson, K., Pursimo, T., Takalo, L. O., et al. 1999, *PASP*, 111, 1223  
Nilsson, K., Pursimo, T., Heidt, J., et al. 2003, *A&A*, 400, 95  
Nilsson, K., Pasanen, M., Takalo, L. O., et al. 2007, *A&A*, 475, 199  
Quinn, J., Akerlof, C. W., Biller, S., et al. 1996, *ApJL*, 456, L83  
Samuelson, F. W., Biller, S. D., Bond, I. H., et al. 1998, *ApJ*, 501, L17  
Scarpa, R., Urry, C., Padovani, P., Calzetti, D., & O'Dowd, M. 2000, *ApJ*, 544, 258  
Sérsic, J.-L. 1968, *Atlas de Galaxias Australes* (Cordoba: Obs. Astron.)  
Shukla, A., Chitnis, V. R., Singh, B. B., et al. 2015, *ApJ*, 798, 2  
Stickel, M., Fried, J. W., & Küehr, H. 1993, *A&AS*, 98, 393  
Urry, C. M., & Padovani, P. 1995, *PASP*, 107, 803  
Urry, C. M., Falomo, R., Scarpa, R., et al. 1998, *ApJ* 512, 88  
Urry, C. M., Scarpa, R., O'Dowd, M., et al. 2000, *ApJ*, 532, 816  
Villata, M., Raiteri, C. M., Lanteri, L., et al. 1998, *A&AS*, 130, 305  
Xie, G. Z., Li, K. H., Zhang, X., Bai, J. M., & Liu, W. W. 1999, *ApJ*, 522, 846  
Xie, G. Z., Li, K. H., Bai, J. M., et al. 2001, *ApJ*, 548, 200  
Xiong, D. R., Zhang, H. J., Zhang, X., et al. 2016, *ApJS*, 222, 24  
Zhang, X., Zhang, L., Zhao, G., et al. 2008, *AJ*, 128, 1929  
Zhang, X., Zheng, Y. G., Zhang, H. J., & Hu, S. M. 2008, *ApJS*, 174, 111